Geophysical Research Letters

RESEARCH LETTER
10.1029/2024GL110792

The Vertical Structure of Turbulence Kinetic Energy Near the Arctic Sea-Ice Surface

Shijie Peng[1], Qinghua Yang[1], Matthew D. Shupe[2,3], Bo Han[1], Dake Chen[1], and Changwei Liu[1]

[1]School of Atmospheric Sciences, Sun Yat-sen University, Southern Marine Science and Engineering Guangdong Laboratory (Zhuhai), Zhuhai, China, [2]Cooperative Institute for Research in Environmental Sciences, University of Colorado Boulder, Boulder, CO, USA, [3]NOAA Physical Science Laboratory, Boulder, CO, USA

Key Points:

- The vertical structures of turbulence kinetic energy (*TKE*) over the Arctic sea-ice surface are investigated using MOSAiC data
- Budget analysis and spectral analysis are used to analyze *TKE* vertical structures near the Arctic sea-ice surface
- The *TKE* vertical structures affect the performance of commonly used turbulence parameterizations

Supporting Information:

Supporting Information may be found in the online version of this article.

Correspondence to:

C. Liu,
liuchw8@mail.sysu.edu.cn

Citation:

Peng, S., Yang, Q., Shupe, M. D., Han, B., Chen, D., & Liu, C. (2024). The vertical structure of turbulence kinetic energy near the Arctic sea-ice surface. *Geophysical Research Letters*, *51*, e2024GL110792. https://doi.org/10.1029/2024GL110792

Received 12 JUN 2024
Accepted 3 NOV 2024

Author Contributions:

Conceptualization: Qinghua Yang, Bo Han, Changwei Liu
Data curation: Matthew D. Shupe, Changwei Liu
Formal analysis: Shijie Peng, Qinghua Yang, Matthew D. Shupe, Dake Chen, Changwei Liu
Funding acquisition: Qinghua Yang, Changwei Liu
Investigation: Shijie Peng, Changwei Liu
Methodology: Shijie Peng, Changwei Liu
Project administration: Qinghua Yang, Bo Han
Resources: Matthew D. Shupe
Supervision: Qinghua Yang, Dake Chen
Validation: Qinghua Yang, Matthew D. Shupe, Dake Chen
Visualization: Shijie Peng, Changwei Liu

Abstract Atmospheric turbulence over the Arctic sea-ice surface has been understudied due to the lack of observational data. In this study, we focus on the turbulence kinetic energy (*TKE*) over sea ice and distinguish its two different vertical structures, the "Surface" type and the "Elevated" type, using observations during the Multidisciplinary drifting Observatory for the Study of Arctic Climate expedition (MOSAiC). The "Surface" type has the maximum *TKE* near the surface (at 2 m), while the "Elevated" type has the maximum *TKE* at a higher level (6 m). The *TKE* budget analysis indicates that the "Elevated" type is caused by the increased shear production of *TKE* at 6 m. In addition, spectral analysis reveals that the contribution to *TKE* by horizontal large eddies is enhanced in the "Elevated" type. Finally, how the vertical structure of *TKE* affects the parameterization of turbulent momentum flux is discussed.

Plain Language Summary In recent years, the Arctic near-surface temperature has increased at a rate that is 3–4 times faster than the global average, which has significant impacts on the global climate. Explaining this phenomenon and predicting future scenarios are urgently needed. Turbulent motions within the Arctic atmospheric boundary layer over the sea-ice surface play an important role in determining near-surface temperature variations, but these turbulent motions and their impacts are not thoroughly understood. To enhance our understanding of the turbulent characteristics of the Arctic boundary layer, the Multidisciplinary drifting Observatory for the Study of Arctic Climate (MOSAiC) was conducted in the central Arctic and collected a wealth of data. Based on the MOSAiC observational data, we investigate the vertical structures of turbulence kinetic energy (*TKE*) in the surface layer and two different vertical structures of *TKE* are distinguished. We then compare the production of *TKE* between these two vertical structures. In addition, we evaluate the performance of parameterization schemes for momentum flux under different vertical *TKE* structures.

1. Introduction

Rapid climate change and declining sea ice in the Arctic have attracted extensive attention (e.g., Esau et al., 2023; Meier & Stroeve, 2022), and the Arctic has entered the "new Arctic" period (Landrum & Holland, 2020). The Arctic atmospheric boundary layer (ABL) plays a crucial role in regulating the interaction between large-scale atmospheric processes and the sea ice, including impacts on sea-ice loss trends and the general Arctic warming (Francis & Hunter, 2006; Graversen et al., 2008). However, turbulent processes in the Arctic ABL have not been thoroughly studied due to a lack of observations, and thus, turbulent flux parameterizations and their adoption in climate models continue to be a grand challenge for the Arctic ABL (e.g., Elvidge et al., 2023; Gryanik et al., 2020; Schneider et al., 2022). Under the backdrop of climate change in the Arctic, it is essential to understand the governing mechanisms of surface turbulent fluxes and improve their representation in numerical models.

With a predominance of near-neutral and stable regimes (Peng et al., 2023; Tjernström et al., 2009), the Arctic ABL generates turbulence mainly through mechanical shear (Grachev et al., 2008). In addition, cloud top cooling (Chechin et al., 2023), wave activity, and submeso-scale motions (Liu et al., 2023) also affect turbulence generation. From the perspective of turbulence production, Mahrt and Vickers (2002) proposed the concepts of "traditional" and "upside-down" boundary layers. The traditional boundary layer is defined as an ABL where turbulence is generated at the surface and transported upward, with constant or decreasing turbulent fluxes with height. In the upside-down boundary layer, in contrast, turbulence is transported downward from a primary source aloft in the boundary layer (e.g., low-level jet, LLJ; Banta et al., 2006, their Figure 1).

Writing – original draft: Shijie Peng, Changwei Liu
Writing – review & editing: Shijie Peng, Qinghua Yang, Matthew D. Shupe, Bo Han, Dake Chen, Changwei Liu

Turbulence kinetic energy (*TKE*) is an important parameter for indicating the amount of turbulence in the ABL and is widely used in the parameterization of turbulent mixing (e.g., Costa et al., 2011; Cuxart et al., 2006; Nakanishi & Niino, 2006). Numerous previous studies investigated *TKE* profiles in the entire ABL (e.g., Banta et al., 2006; Lan et al., 2018; Mahrt, 2014). In general, the *TKE* decreases with height for the weakly stable regime, while *TKE* increases with height and reaches a maximum near the nose of the LLJ for the very stable regime. However, few studies have focused on the details of the near-surface vertical *TKE* structure. In the atmospheric surface layer with weak winds, turbulence collapses near the surface with a small *TKE*, referred to as the "decoupled" state. When near-surface wind speed increases over a critical value, *TKE* significantly increases, and turbulence couples with the surface (Lan et al., 2018; Sun et al., 2012). For the Arctic near-surface layer, the *TKE* structure significantly influences atmosphere-sea ice interactions. However, measurements of turbulence over the Arctic sea-ice surface are sparse, leading to a limited understanding of turbulent motions in this area.

The recent expedition named the Multidisciplinary drifting Observatory for the Study of Arctic Climate (MOSAiC, from October 2019 to September 2020) fills this critical research gap. The MOSAiC expedition collected a wealth of observational data, including near-surface turbulence observations (Cox et al., 2023; Shupe et al., 2022). These data contribute to more comprehensive studies of the near surface TKE characteristics of the Arctic ABL. In this study, we aim to reveal the vertical structures of near-surface *TKE* and investigate their controlling factors. We also aim to evaluate how the vertical structures of *TKE* affect the performance of commonly used turbulence parameterization schemes. In the following, data and methods are described in Section 2 and results and discussion are presented in Section 3. Summary are given in Section 4.

2. Data and Methods

2.1. Observational Data

During MOSAiC, turbulence data were collected on a 10-m meteorological tower installed on the sea-ice surface at the "Met City", which was located 300–600 m away from the research vessel *Polarstern* as it drifted passively with the sea ice (Cox et al., 2023). The year-round turbulence data set had two significant interruptions (i.e., from 10 May to 24 Jun 2020 and from 29 Jul to 25 Aug 2020) when the research vessel was underway for logistical reasons. The specific drift track has been presented elsewhere (Liu et al., 2023, see their Figure 1). All measured turbulence data are considered here, and the data are not subsetted based on season, sea ice fraction or cloud conditions. Eddy-covariance measurements (three-dimensional wind velocity components and sonic temperature) were made at nominal heights of 2, 6, and 10 m on the tower with u-Sonic-3 Cage MP anemometers (METEK GmbH, Germany). The sampling frequency of the anemometer is 20 Hz, resampled to 10 Hz. The EC data are processed in 10-min blocks, and error flag detection, despiking, true wind correction, and coordinate rotation via double rotation are performed to derive turbulence quantities (e.g., *TKE* and momentum flux).

2.2. TKE Budget Analysis

After confirming very limited Coriolis effects below 10 m by checking the wind direction, we use a coordinate system aligned with the mean wind and assume zero subsidence. A simplified form of the *TKE* budget equation is (e.g., Kaimal & Finnigan, 1994; Stull, 1988):

$$\underbrace{\frac{\partial \overline{e}}{\partial t}}_{S_{tg}} = \underbrace{-\overline{u}\frac{\partial \overline{e}}{\partial x}}_{A} \underbrace{+g\frac{}{\overline{\theta_v}}\overline{w'\theta_v'}}_{B} \underbrace{-\overline{u'w'}\frac{\partial \overline{u}}{\partial z}}_{S_{hr}} \underbrace{-\frac{\partial \overline{w'e}}{\partial z}}_{T_t} \underbrace{-1\frac{}{\overline{\rho}}\frac{\partial \overline{w'p'}}{\partial z}}_{T_p} \underbrace{-\varepsilon}_{D} . \quad (1)$$

In this *TKE* budget equation, S_{tg} represents the local storage of *TKE*, A is the advection term, B is the buoyancy production/consumption term, S_{hr} represents the production by mechanical shear, T_t is the turbulent transport term, T_p is the pressure transport term, and D represents the viscous dissipation of *TKE*. The A and T_p terms cannot be calculated directly due to many difficulties involved in measurements and are considered as the residual term (R). The specific description and normalization of Equation 1 is given in Text S1 in Supporting Information S1.

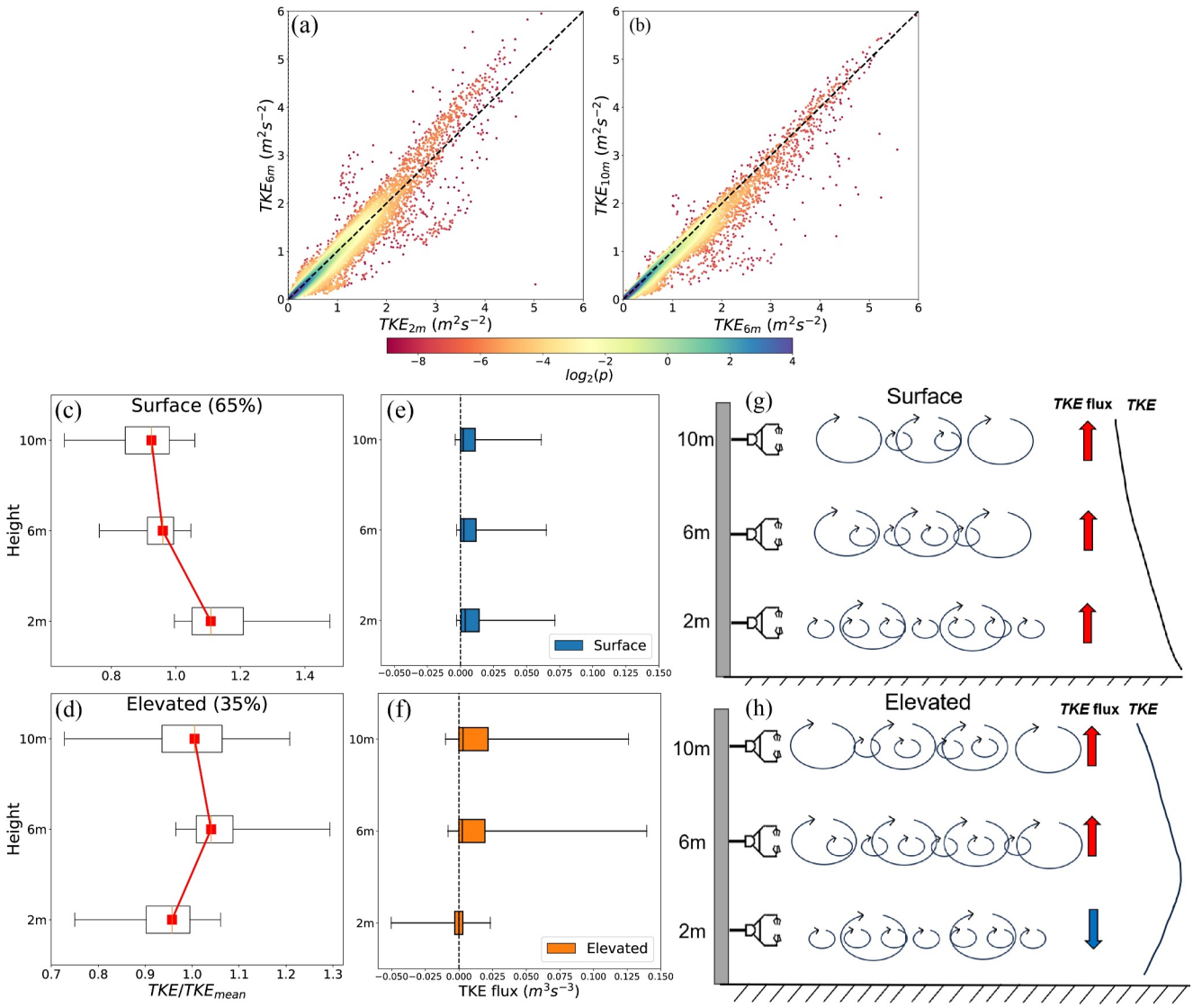

Figure 1. (a, b) Comparison of *TKE* values at different levels (2, 6, and 10 m). The points are colored by $\log_2(p)$, where p is the kernel-density estimate calculated by Gaussian kernels. (c, d) Vertical profiles of normalized *TKE* for the "Surface" and "Elevated" structural types. TKE_{mean} is a scalar value (i.e., the mean value of *TKE* at three levels). (e, f) Box-and-whisker plots of *TKE* flux at three levels for the two *TKE* structural types. The whiskers, the boxes, and the horizontal black lines show the 5th, 25th, 50th, 75th, and 95th percentile values. (g, h) The schematic illustration for explaining the two different *TKE* structures. The large and small circles represent large- and small-scale turbulent eddies, respectively. The number of eddies is used to represent the spectral densities of eddies. The red and blue arrows represent upward and downward *TKE* flux, respectively. The solid black lines show the vertical *TKE* profiles.

3. Results and Discussion

3.1. Vertical Structures of Near-Surface TKE

Figures 1a and 1b present the comparisons of *TKE* values at 2-m (TKE_{2m}), 6-m (TKE_{6m}), and 10-m (TKE_{10m}) heights. For *TKE* values less than about 3 $m^2\ s^{-2}$, the data shown in Figure 1a are uniformly distributed on both sides of the 1:1 line, which means that the occurrences of $TKE_{2m} > TKE_{6m}$ and $TKE_{2m} < TKE_{6m}$ are almost equal. In contrast, the data in Figure 1b are concentrated on the right side of the 1:1 line, that is, TKE_{6m} is usually larger than TKE_{10m}. Therefore, we use the ratio of TKE_{6m} to TKE_{2m} ($R_{TKE} = TKE_{6m}/TKE_{2m}$) to divide these cases into two categories: $R_{\mathrm{TKE}} < 1$ and $R_{\mathrm{TKE}} > 1$. Figures 1c and 1d present the *TKE* statistics at three levels normalized by a single scalar value TKE_{mean} (i.e., the mean value of *TKE* at three levels), representing vertical structures of near-surface *TKE* of these two categories. The *TKE* statistics normalized by u_*^2 are also presented in Figure S2 in Supporting Information S1. The structure with $R_{\mathrm{TKE}} < 1$ (Figure 1c) accounts for 65% of the total samples,

characterized by a maximum *TKE* at the 2-m level and *TKE* decreasing with height. The cases of $R_{\mathrm{TKE}} > 1$ (Figure 1d) account for 35% of the total samples, with the maximum *TKE* located at the 6-m level. For convenience, we call these two *TKE* vertical structures the "Surface" type and the "Elevated" type, respectively. The seasonal statistics of the "Surface" and "Elevated" types are presented in Figure S3 in Supporting Information S1. The "Elevated" type occurs more frequently during the spring season, while the "Surface" type dominates in the other three seasons.

To further illustrate the characteristics of these two structural types, the *TKE* flux ($\overline{w'e}$) statistics are presented in Figures 1e and 1f. For the "Surface" type, positive *TKE* flux dominates across all three levels, which means that turbulence is mainly generated near the surface and transported upward. This profile is consistent with our traditional understanding of weakly stable boundary layers (Mahrt, 2014) or "traditional" boundary layers (Mahrt & Vickers, 2002). For the "Elevated" type, the positive *TKE* fluxes at the 6-m and 10-m levels have a larger range than that for the "Surface" type, while the *TKE* flux at 2-m is weak and periodic downward. Upward transport of *TKE* above the 6-m level and periodic downward transport of *TKE* at the 2-m level indicates that the principal source of turbulence is not at the surface, but detached from the surface (i.e., elevated to near the 6-m level). Figures 1g and 1h give schematic illustrations of these two near-surface *TKE* structural types and *TKE* flux directions.

3.2. TKE Budget Analysis and Relevant Factors

In this section, we analyze the two different *TKE* vertical structures through the normalized *TKE* budget equation (Equation S3 in Supporting Information S1). The statistics of the *TKE* budget terms at three levels for the "Surface" type (Figure 2a) and the "Elevated" type (Figure 2b) are presented. Generally, the buoyancy term (B) and the local storage term (not shown) are at least an order of magnitude smaller than the other terms and, therefore, can be neglected. The shear production term (S_{hr}) and the dissipation term (D) are the largest and roughly form a local equilibrium. These results indicate that mechanical shear is the dominant mechanism for generating turbulence near the surface, and the effect of buoyancy is negligible, possibly due to the lack of stratification.

By comparing the *TKE* budget terms under two different *TKE* vertical structure types, we find that the significant differences between them are in the S_{hr} term and the D term at the 6-m level. The 6-m S_{hr} in the "Elevated" type is generally higher than that in "Surface" cases. The D term in the "Elevated" type is excess at 2-m height and decreases more strongly than S_{hr} term at 6 and 10 m, leading to significant residual terms (R), that may represent the pressure transport term (Högström et al., 2002). In addition, the vertical transport term (T_t) in the "Elevated" type has a slightly negative contribution at the 2-m level, consistent with the *TKE* flux statistics (see Figure 1f). These significant transport terms and residual terms indicate that *TKE* in "Elevated" cases is locally imbalanced, with strong redistribution processes.

We further compare the S_{hr} term in these two types, as it is the dominant *TKE* production. The S_{hr} in the "Surface" type decreases with height, while S_{hr} in the "Elevated" type, in contrast, roughly remains constant between 2 and 6 m, and the maximum of S_{hr} occurs at 6 m in some cases. The S_{hr} profiles for the "Surface" and "Elevated" cases correspond with their respective vertical *TKE* structures in Figures 1c and 1d. According to Equation 1, the S_{hr} term is dependent on the interaction of vertical momentum flux ($\overline{u'w'}$) and vertical gradient of the horizontal wind ($\frac{\partial \overline{u}}{\partial z}$, S), so we calculate the ratio of $\overline{u'w'}$ at 6 m to that at 2 m ($R_{\overline{u'w'}} = \overline{u'w'}_{6\mathrm{m}} / \overline{u'w'}_{2\mathrm{m}}$) and the ratio of S at 6 m to that at 2 m ($R_s = S_{6m}/S_{2m}$). The distributions of these two ratios are presented in Figures 2c and 2d. It can be found that the main difference is in $R_{\overline{u'w'}}$ distributions, with $\overline{u'w'}$ remaining constant or increasing with height in "Elevated" cases. In comparison, the vertical gradients of wind speed are similar in "Surface" and "Elevated" cases (see also wind profile statistics shown in Figure S4 in Supporting Information S1). We also present $R_{\overline{u'w'}}$ and R_s distributions under different stability parameter (z/L, where L is the Obukhov length) and obtain similar results (Figure S5 in Supporting Information S1). These results indicate that the unique S_{hr} profile in "Elevated" cases is attributed to the impact of $\overline{u'w'}$, rather than the vertical gradient of wind speed. These results are consistent with the *TKE* budget characteristics over a heterogeneous surface (Babić et al., 2018). Therefore, we hypothesize that the "Elevated" *TKE* profiles are triggered by surface heterogeneity.

Here we give more evidences to support this heterogeneity hypothesis. The surface heterogeneity in the Arctic is characterized by ridges, vertical edges of ice floes and melt ponds, etc., and is associated with sea ice fraction

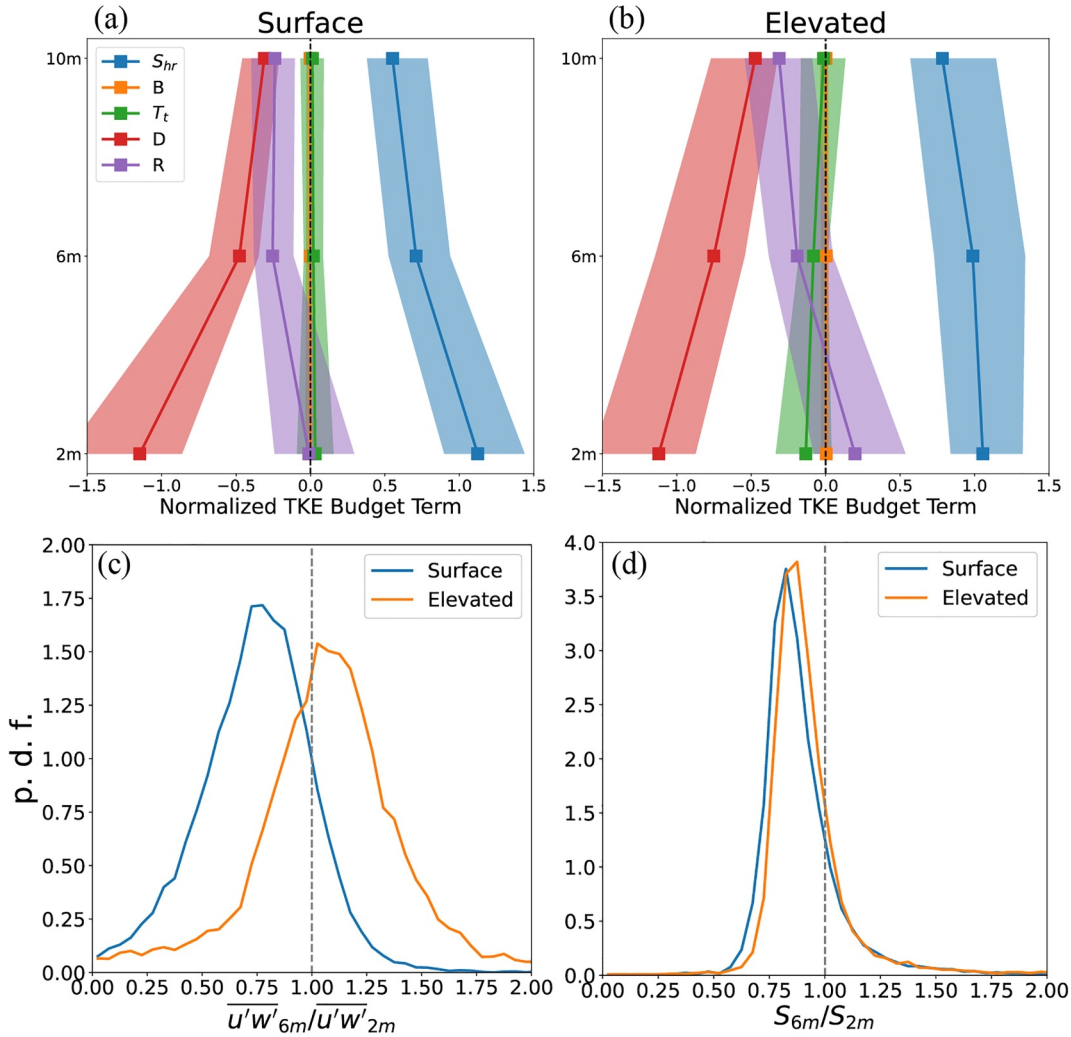

Figure 2. The normalized *TKE* budget terms at three levels (2, 6, and 10 m) in (a) "Surface" and (b) "Elevated" cases. The shading and symbols show the 25th, 50th, and 75th percentile values. The probability density functions (p. d. f.) of ratios of (c) vertical momentum flux and (d) vertical gradient of the horizontal wind at 6-m level to 2-m level. The blue and orange lines represent the "Surface" and "Elevated" cases, respectively.

(Andreas et al., 2010; Elvidge et al., 2021; Lüpkes & Birnbaum, 2005). We present the occurrence frequencies of the "Surface" and "Elevated" cases under different sea ice fractions (Figure S6 in Supporting Information S1). The results show that the "Elevated" type occurs more frequently at ice fractions of 0.8–0.9, which could be attributed to the ice floe edges in the marginal ice zones (Elvidge et al., 2021) and explain the seasonal statistical characteristics of "Elevated" cases (i.e., Figure S3 in Supporting Information S1). Additionally, we present the 2-m wind direction distribution of the two structural types (Figure S7 in Supporting Information S1). The results show that wind direction in "Surface" cases is distributed approximately uniformly, while northwest winds and southeast winds dominate in "Elevated" cases. The preferred wind directions in "Elevated" cases imply the potential role of surface heterogeneity upstream. More topographic data are required to validate this hypothesis in future work.

3.3. Case Study: The Spectra of TKE and Its Horizontal and Vertical Components

Selected cases are used to further illustrate the "Surface" and "Elevated" structural types and their differences. We select a period of 7 May 2020, 04:00–15:00 UTC, when the *TKE* structure transitioned from the typical "Surface" type to the "Elevated" type. The surface layer during this period remains under near-neutral regime ($-0.01 < z/L < 0$). Figure S8 in Supporting Information S1 presents the time series of near-surface wind speed, wind direction, *TKE*, R_{TKE}, and turbulence intensity (σ_U/U). In this case, the wind speed and *TKE* values show a slightly

upward trend. R_{TKE} rises over 1.0 at 09:40 UTC, marking the transition time between the "Surface" and "Elevated" types. Significant decrease in wind direction angles indicates a change in the flux footprint. The difference of turbulence intensity at the 2-m and 6-m levels narrows with increasing 6-m turbulence intensity. Thus, the near-surface vertical structure of *TKE* follows the "Surface" type in Period 1 (04:00–09:40 UTC) and the "Elevated" type in Period 2 (09:40–15:00 UTC).

We perform a Fourier transform on each data block with the number of points that are a power of 2 (about 13 min) and then calculate the quantile *TKE* spectra (25th, 50th, and 75th percentiles) during Period 1 and Period 2 (Figures 3a and 3b). For the *TKE* spectra under the "Surface" state, stronger contributions of small eddies (frequency, $f > 0.1$ Hz) occur at 2 m than at 6 m. Meanwhile, the low-frequency turbulence spectra at 2 and 6 m are close. For the "Elevated" state, in contrast, the *TKE* spectrum at 2 m is similar to that of the 2-m "Surface" type in magnitude, while the 6-m TKE spectrum significantly increases in both low- and high-frequency components. The 6-m quantile *TKE* spectra (50th and 75th percentiles) show a peak in the low-frequency range ($f \approx 0.01$ Hz), and this peak is possibly attributed to the contribution of large-scale turbulent eddies (Lan et al., 2019), since nonturbulent submeso-scale motions typically occur under stable conditions (Acevedo et al., 2014; Vercauteren et al., 2016), and their frequency is an order of magnitude less than 0.01 Hz in the polar ABL (Cava et al., 2019; Liu et al., 2023). The large eddies further force the small eddies at the 6-m level through energy cascade, thereby making the high-frequency spectrum at 6 m closer to that at 2 m and leading to an overall *TKE* increase at 6 m. The schematic illustrations of large and small eddies at three heights in the "Surface" and "Elevated" types are presented in Figures 1g and 1h, respectively.

We further analyze the impacts of horizontal and vertical flows on the *TKE* by presenting the quantile spectra of horizontal and vertical components of wind speed (S_{uu} and S_{ww}, shown in Figures 3c and 3d. The results show that the variation of S_{uu} spectra from the "Surface" state to "Elevated" state is also similar to that of *TKE* spectra, with the enhanced 6-m "Elevated" S_{uu} spectrum at low-frequency range and narrowed difference in high-frequency spectra between the 2-m level and 6-m level. In contrast, the variation of S_{ww} spectra from the two states is distinct from the others. Through the energy cascade, at low-frequency range the 6-m S_{ww} spectrum hardly changes, while at the high the spectrum increases. These results indicate that large-scale eddies are mainly dominated by horizontal flow. These results can also be explained by surface heterogeneity. Fesquet (2008) and Fesquet et al. (2009) have confirmed the link between large eddies and heterogeneity experimentally and numerically. The inactive large eddies are created and developed above the heterogeneous surface, that are hereafter transported downward and impinge onto the ground, and active small eddies are generated through this "top-down" mechanism. This mechanism can also explain the excess turbulence dissipation at 2-m height and *TKE* budget imbalance as mentioned in Sect. 3.2 (Högström et al., 2002).

3.4. Effects of the TKE Structures on Parameterizing Near-Surface Momentum Flux

In this section, we focus on the commonly used 1.5-order *TKE*-based turbulence closure in the planetary boundary layer schemes as used in large scale and mesoscale weather prediction and climate models and discuss the effects of different *TKE* structures on parameterizing near-surface momentum flux. It should be noted that the "Surface" and "Elevated" types discussed here are simplified three-level *TKE* structures, and based on the available measurements we do not have further information on the small-scale vertical distribution of *TKE*. In the standard turbulence closure model, the momentum flux is parameterized as:

$$\overline{u'w'} = -v_M S, \tag{2}$$

where v_M is the eddy viscosity, and S is the vertical gradient of mean streamwise velocity component. The 1.5-order schemes estimate the eddy viscosity (v_M) based on the *TKE* (e) and a turbulent mixing length scale (l_K):

$$v_M = l_K \sqrt{e}. \tag{3}$$

In the surface layer under the near-neutral regime, l_K is expressed as (Redelsperger et al., 2001):

$$l_K = \frac{1}{\sqrt{\alpha}} \kappa z, \tag{4}$$

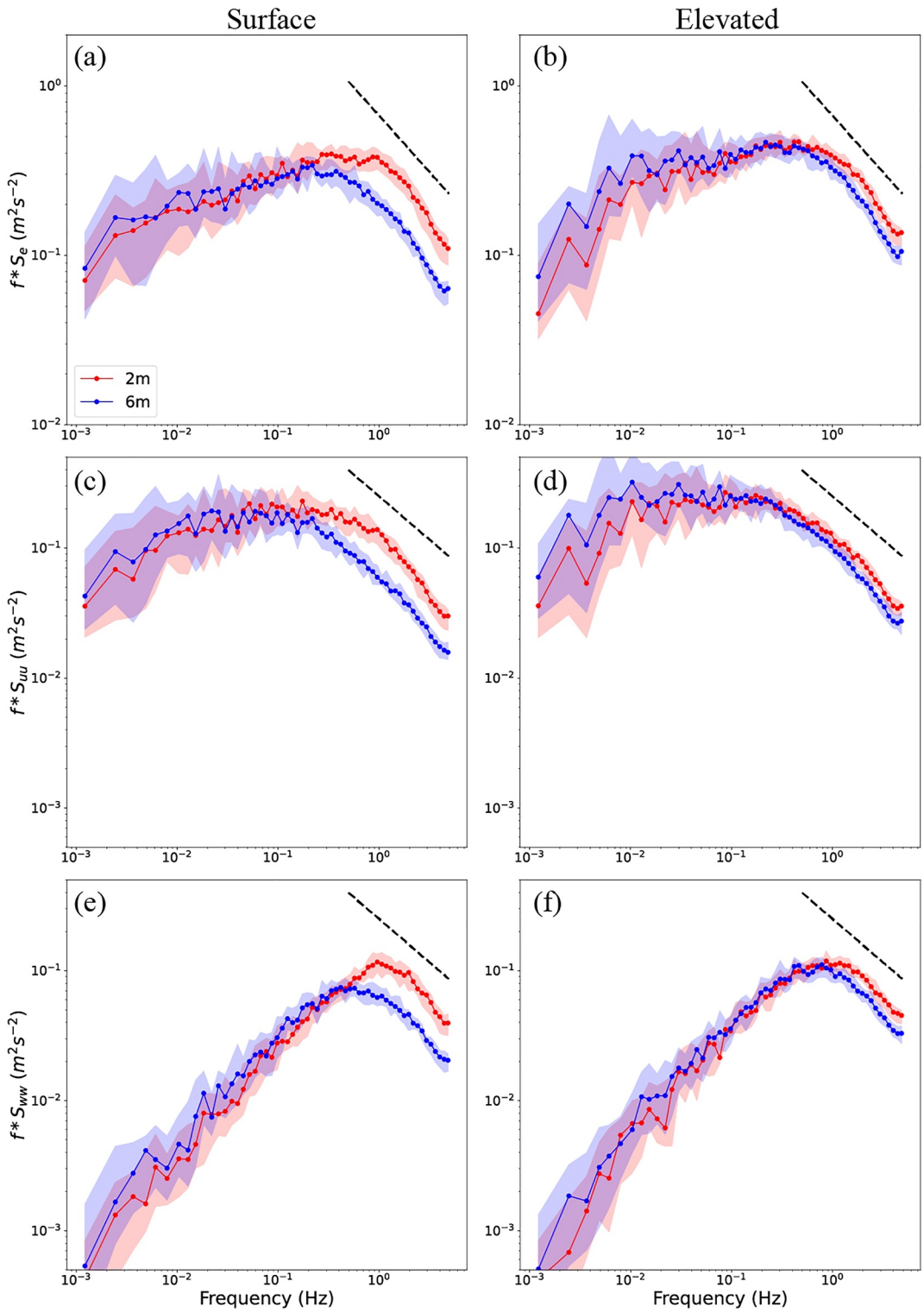

Figure 3. The spectra of *TKE* (upper panels) and its horizontal component (S_{uu}; middle panels) and vertical component (S_{ww}; lower panels) for the "Surface" state (left panels) and "Elevated" state (right panels). The quantile spectra for "Surface" and "Elevated" states are calculated for the Period 1 and Period 2 in Figure S8 of Supporting Information S1, respectively. The shading and symbols show the 25th, 50th, and 75th percentile values. Red and blue colors represent 2-m and 6-m levels, respectively.

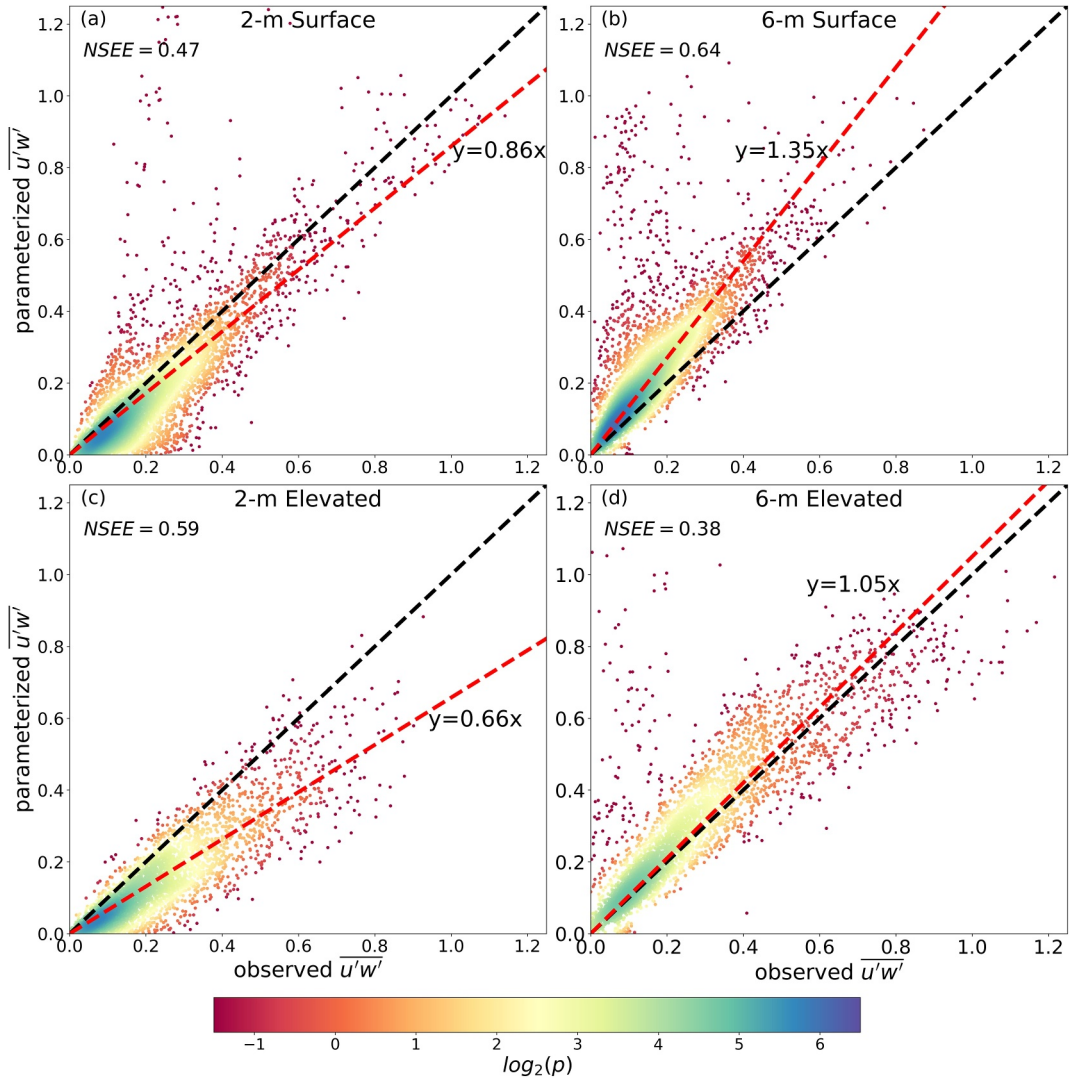

Figure 4. Comparisons of near-surface momentum fluxes between the simulations and observations for "Surface" (upper panels) and "Elevated" (lower panels) cases. Only near-neutral cases are selected. Left panels and right panels show momentum fluxes at 2-m and 6-m levels, respectively. The points are colored by $\log_2(p)$, where p is the kernel-density estimate calculated by Gaussian kernels. The red dashed lines are the best-fit line, and the black dashed lines are the 1:1 line. The normalized standard error (*NSEE*) is given in each panel.

where $\alpha = 4.63$ theoretically derived by Redelsperger et al. (2001). It should be noted that Equation 4 is available for the surface layer (i.e., the bottom ~10% of the boundary layer). According to Peng et al. (2023), the annual average height of the Arctic boundary layer is 231 m. To ensure that the evaluated layer is indeed the surface layer, we exclude cases with boundary layer height less than 100 m (accounting for about 10%).

We select the near-neutral cases ($-0.01 < z/L < 0.01$; accounting for 42%) and calculate the parameterized $\overline{u'w'}$ based on Equations 2–4 for "Surface" and "Elevated" cases. The comparisons between observed $\overline{u'w'}$ and parameterized $\overline{u'w'}$ are shown in Figure 4, where best-fit curves and the normalized standard error (*NSEE*; same as Xi et al., 2024) are also given. The results suggest that for the "Surface" cases, the parameterized $\overline{u'w'}$ corresponds well with the observed $\overline{u'w'}$ at the 2-m level, with the slope of best-fit line of 0.86. However, the parameterization for 6-m "Surface" cases overestimate $\overline{u'w'}$, and the slope of best-fit line is 1.35. For the "Elevated" cases, the parameterization results present significant underestimation at the 2-m level, with the slope of the best fit line of 0.66 and *NSEE* = 0.59, while at the 6-m level the best-fit line is closest to the 1-to-1 reference line with a slope of 1.05 and the lowest *NSEE* of 0.38. These results suggest that near-surface momentum flux can be better

reproduced by Equations 2–4 at the height of maximum *TKE*, and the height-dependent l_K expression Equation 4 is more suitable near the height closest to the turbulence source.

We also evaluate the $\overline{u'w'}$ parameterization schemes under stratified conditions (including stable and unstable regimes) by selecting the cases with z/L larger than 0.01 and less than 0.01, respectively. The l_K expression adds a stability function in stratified surface layers, and the details are presented in Text S2 in Supporting Information S1. The results are shown in Figures S9 and S10 in Supporting Information S1. Overall, the parameterization schemes present larger deviations under stable and unstable regimes compared with the results in near-neutral conditions, especially for stable cases. But, similar to the results shown in near-neutral conditions, significant overestimation and underestimation occurs for 6-m "Surface" cases and 2-m "Elevated" cases under stratified conditions, respectively. Climate models usually use a long-tail stability function into near-surface turbulence parameterization to improve the representation of large-scale flow and near-surface temperature, but it causes the overestimation of *TKE* (Sandu et al., 2013), which fits the results of "Surface" cases. Including the "Elevated" *TKE* cases in models could be helpful to improve the representation of orographic drag and solve this problem. Specifically, roughness length has an impact on mixing length scale (l_K) and can be taken into account.

4. Summary and Future Work

Using turbulence data obtained from the MOSAiC expedition, we investigate the vertical structure of near-surface *TKE* and its controlling factors. The vertical structures of near-surface *TKE* are divided into the "Surface" and "Elevated" types based on comparisons of *TKE* at three levels. In "Elevated" cases, the source of *TKE* generation is not at the surface but elevated to around the 6-m level. *TKE* budget analysis suggests that mechanical shear plays a dominant role in generating turbulence. The elevated *TKE* source in the "Elevated" structure is attributed to the significant increase of mechanical shear generation at the 6-m level, associated with increased $\overline{u'w'}$ at the 6-m level. Significant *TKE* budget imbalance leads to the surface heterogeneity hypothesis. The preferences for sea ice fractions and wind directions in the "Elevated" cases further support this hypothesis. Spectral analysis indicates that the contribution of horizontal large eddies to *TKE* is enhanced at the 6-m level for the "Elevated" type relative to the "Surface" type, which also translates to a higher contribution of small eddies through the energy cascade, leading to an overall TKE increase at 6 m. These results are consistent with the "top-down" mechanism (Fesquet et al., 2009), with large eddies possibly created above the heterogeneous surface.

We further evaluate commonly used 1.5-order *TKE*-based parameterization schemes under different *TKE* structures. The results indicate that for this observational data set $\overline{u'w'}$ can be better reproduced at the height closest to the strong *TKE* source, that is, the mixing length scale (l_K) is more reasonable at the 2-m "Surface" cases and 6-m "Elevated" cases. The l_K parameterization can be improved to include "Elevated" *TKE* cases in meteorological models, which could be helpful for representation of orographic drag in polar regions.

This study improves the understanding of vertical structures of near-surface *TKE* over the Arctic sea-ice surface and hypotheses the topographic contribution. However, more observational data are needed to validate these findings over a wider range of conditions. Future work on representing spatiotemporal variability in the topography of sea ice and confirming the connection between the "Elevated" cases and heterogeneity to improve turbulent flux parameterizations in meteorological models is recommended.

Data Availability Statement

All MOSAiC surface flux and turbulent data are available at the Arctic Data Center via Cox et al. (2023).

Acknowledgments
Data used in this manuscript were produced as part of the international Multidisciplinary drifting Observatory for the Study of Arctic Climate (MOSAiC) expedition with tag MOSAiC20192020. We greatly appreciate Professor Dan Li from Boston University for the constructive comments to this study. We also thank all persons involved in the expedition of the Research Vessel Polarstern during MOSAiC in 2019–2020 (AWI_PS122_00) as listed in Nixdorf et al. (2021). The University of Colorado/NOAA surface flux team is acknowledged for the efforts in collecting and post-processing the near-surface flux and meteorological measurements. This study was supported by the National Key Research and Development Program of China (No. 2022YFE0106300), the Fengyun-3 (03) Batch Meteorological Satellite Project (FY-3 (03) -AS-11.10-ZT, FY-3 (03) -AS-11.12-ZT), the Southern Marine Science and Engineering Guangdong Laboratory (Zhuhai) (Nos. SML2023SP217, SML2023SP219, SML2022SP401), and the National Natural Science Foundation of China (No. 42105072). MDS was supported by the US National Science Foundation (OPP-1724551), DOE Atmospheric System Research Program (DE-SC0023036), NOAA Global Ocean Monitoring and Observing Program (FundRef https://doi.org/10.13039/100018302), and NOAA Physical Sciences Laboratory (NA22OAR4320151).

References

Acevedo, O. C., Costa, F. D., Oliveira, P. E. S., Puhales, F. S., Degrazia, G. A., & Roberti, D. R. (2014). The influence of submeso processes on stable boundary layer similarity relationships. *Journal of the Atmospheric Sciences*, *71*(1), 207–225. https://doi.org/10.1175/JAS-D-13-0131.1

Andreas, E. L., Horst, T. W., Grachev, A. A., Persson, P. O. G., Fairall, C. W., Guest, P. S., & Jordan, R. E. (2010). Parametrizing turbulent exchange over summer sea ice and the marginal ice zone. *Quarterly Journal of the Royal Meteorological Society*, *136*(649), 927–943. https://doi.org/10.1002/qj.618

Babić, K., & Rotach, M. W. (2018). Turbulence kinetic energy budget in the stable boundary layer over a heterogeneous surface. *Quarterly Journal of the Royal Meteorological Society*, *144*(713), 1045–1062. https://doi.org/10.1002/qj.3274

Banta, R. M., Pichugina, Y. L., & Brewer, W. A. (2006). Turbulent velocity-variance profiles in the stable boundary layer generated by a nocturnal low-level jet. *Journal of the Atmospheric Sciences*, *63*(11), 2700–2719. https://doi.org/10.1175/JAS3776.1

Cava, D., Mortarini, L., Anfossi, D., & Giostra, U. (2019). Interaction of submeso motions in the Antarctic stable boundary layer. *Boundary-Layer Meteorology*, *171*(2), 151–173. https://doi.org/10.1007/s10546-019-00426-7

Chechin, D. G., Lüpkes, C., Hartmann, J., Ehrlich, A., & Wendisch, M. (2023). Turbulent structure of the Arctic boundary layer in early summer driven by stability, wind shear and cloud-top radiative cooling: ACLOUD airborne observations. *Atmospheric Chemistry and Physics*, *23*(8), 4685–4707. https://doi.org/10.5194/acp-23-4685-2023

Costa, F. D., Acevedo, O. C., Mombach, J. C. M., & Degrazia, G. A. (2011). A simplified model for intermittent turbulence in the nocturnal boundary layer. *Journal of the Atmospheric Sciences*, *68*(8), 1714–1729. https://doi.org/10.1175/2011JAS3655.1

Cox, C., Gallagher, M., Shupe, M. D., Persson, O., Blomquist, B., Grachev, A., et al. (2023). Met city meteorological and surface flux measurements (level 3 final), multidisciplinary drifting observatory for the study of Arctic climate (MOSAiC), central Artic, October 2019 - September 2020 [Dataset]. *NSF Arctic Data Center*. https://doi.org/10.18739/A2TM7227K

Cuxart, J., Holtslag, A. A. M., Beare, R. J., Bazile, E., Beljaars, A., Cheng, A., et al. (2006). Single-column model intercomparison for a stably stratified atmospheric boundary layer. *Boundary-Layer Meteorology*, *118*(2), 273–303. https://doi.org/10.1007/s10546-005-3780-1

Elvidge, A. D., Renfrew, I. A., Brooks, I. M., Srivastava, P., Yelland, M. J., & Prytherch, J. (2021). Surface heat and moisture exchange in the marginal ice zone: Observations and a new parameterization scheme for weather and climate models. *Journal of Geophysical Research: Atmospheres*, *126*(17), e2021JD034827. https://doi.org/10.1029/2021JD034827

Elvidge, A. D., Renfrew, I. A., Edwards, J. M., Brooks, I. M., Srivastava, P., & Weiss, A. I. (2023). Improved simulation of the polar atmospheric boundary layer by accounting for aerodynamic roughness in the parameterization of surface scalar exchange over sea ice. *Journal of Advances in Modeling Earth Systems*, *15*(3), e2022MS003305. https://doi.org/10.1029/2022MS003305

Esau, I., Pettersson, L. H., Cancet, M., Chapron, B., Chernokulsky, A., Donlon, C., et al. (2023). The Arctic amplification and its impact: A synthesis through satellite observations. *Remote Sensing*, *15*(5), 1354. https://doi.org/10.3390/rs15051354

Fesquet, C. (2008). *Structure de la turbulence atmosphérique à proximité de la surface. (Doctoral dissertation)*. Ecole Polytechnique.

Fesquet, C., Dupont, S., Drobinski, P., Dubos, T., & Barthlott, C. (2009). Impact of terrain heterogeneity on coherent structure properties: Numerical approach. *Boundary-Layer Meteorology*, *133*(1), 71–92. https://doi.org/10.1007/s10546-009-9412-4

Francis, J. A., & Hunter, E. (2006). New insight into the disappearing Arctic sea ice. *Eos, Transactions American Geophysical Union*, *87*(46), 509–511. https://doi.org/10.1029/2006EO460001

Grachev, A. A., Andreas, E. L., Fairall, C. W., Guest, P. S., & Persson, P. O. G. (2008). Turbulent measurements in the stable atmospheric boundary layer during SHEBA: Ten years after. *Acta Geophysica*, *56*(1), 142–166. https://doi.org/10.2478/s11600-007-0048-9

Graversen, R. G., Mauritsen, T., Tjernström, M., Kallen, E., & Svensson, G. (2008). Vertical structure of recent Arctic warming. *Nature*, *451*(7174), 53–56. https://doi.org/10.1038/nature06502

Gryanik, M. V., Lüpkes, C., Grachev, A., & Sidorenko, D. (2020). New modified and extended stability functions for the stable boundary layer based on SHEBA and parametrizations of bulk transfer coefficients for climate models. *Journal of the Atmospheric Sciences*, *77*(8), 2687–2716. https://doi.org/10.1175/JAS-D-19-0255.1

Högström, U., Hunt, J. C. R., & Smedman, A.-S. (2002). Theory and measurements for turbulence spectra and variances in the atmospheric neutral surface layer. *Boundary-Layer Meteorology*, *103*(1), 101–124. https://doi.org/10.1023/A:1014579828712

Kaimal, J. C., & Finnigan, J. J. (1994). *Atmospheric boundary layer flows: Their structure and measurements*. Oxford University Press.

Lan, C., Liu, H., Katul, G. G., Li, D., & Finn, D. (2019). Large eddies regulate turbulent flux gradients in coupled stable boundary layers. *Geophysical Research Letters*, *46*(11), 6090–6100. https://doi.org/10.1029/2019GL082228

Lan, C., Liu, H., Li, D., Katul, G. G., & Finn, D. (2018). Distinct turbulence structures in stably stratified boundary layers with weak and strong surface shear. *Journal of Geophysical Research: Atmospheres*, *123*(15), 7839–7854. https://doi.org/10.1029/2018JD028628

Landrum, L., & Holland, M. M. (2020). Extremes become routine in an emerging new Arctic. *Nature Climate Change*, *10*(12), 1108–1115. https://doi.org/10.1038/s41558-020-0892-z

Liu, C., Yang, Q., Shupe, M. D., Ren, Y., Peng, S., Han, B., & Chen, D. (2023). Atmospheric turbulent intermittency over the Arctic sea-ice surface during the MOSAiC expedition. *Journal of Geophysical Research: Atmospheres*, *128*(15), e2023JD038639. https://doi.org/10.1029/2023JD038639

Lüpkes, C., & Birnbaum, G. (2005). Surface drag in the Arctic marginal sea-ice zone: A comparison of different parameterisation concepts. *Boundary-Layer Meteorology*, *117*(2), 179–211. https://doi.org/10.1007/s10546-005-1445-8

Mahrt, L. (2014). Stably stratified atmospheric boundary layers. *Annual Review of Fluid Mechanics*, *46*(1), 23–45. https://doi.org/10.1146/annurev-fluid-010313-141354

Mahrt, L., & Vickers, D. (2002). Contrasting vertical structures of nocturnal boundary layers. *Boundary-Layer Meteorology*, *105*(2), 351–363. https://doi.org/10.1023/A:1019964720989

Meier, W. N., & Stroeve, J. (2022). An updated assessment of the changing Arctic sea ice cover. *Oceanography*, *35*, 10–19. https://doi.org/10.5670/oceanog.2022.114

Nakanishi, M., & Niino, H. (2006). An improved Mellor–Yamada level-3 model: Its numerical stability and application to a regional prediction of advection fog. *Boundary-Layer Meteorology*, *119*(2), 397–407. https://doi.org/10.1007/s10546-005-9030-8

Nixdorf, U., Dethloff, K., Rex, M., Shupe, M., Sommerfeld, A., Perovich, D. K., et al. (2021). *MOSAiC Extended Acknowledgement*. Zenodo. https://doi.org/10.5281/ZENODO.5541624

Peng, S., Yang, Q., Shupe, M. D., Xi, X., Han, B., Chen, D., et al. (2023). The characteristics of atmospheric boundary layer height over the Arctic Ocean during MOSAiC. *Atmospheric Chemistry and Physics*, *23*(15), 8683–8703. https://doi.org/10.5194/acp-23-8683-2023

Redelsperger, J. L., Mahe, F., & Carlotti, P. (2001). A simple and general subgrid model suitable both for surface layer and free-stream turbulence. *Boundary-Layer Meteorology*, *101*(3), 375–408. https://doi.org/10.1023/A:1019206001292

Sandu, I., Beljaars, A., Bechtold, P., Mauritsen, T., & Balsamo, G. (2013). Why is it so difficult to represent stably stratified conditions in numerical weather prediction (NWP) models? *Journal of Advances in Modeling Earth Systems*, *5*(2), 117–133. https://doi.org/10.1002/jame.20013

Schneider, T., Lüpkes, C., Dorn, W., Chechin, D., Handorf, D., Khosravi, S., et al. (2022). Sensitivity to changes in the surface-layer turbulence parameterization for stable conditions in winter: A case study with a regional climate model over the Arctic. *Atmospheric Science Letters*, *23*(1), e1066. https://doi.org/10.1002/asl.1066

Shupe, M. D., Rex, M., Blomquist, B., Persson, P. O. G., Schmale, J., Uttal, T., et al. (2022). Overview of the MOSAiC expedition-atmosphere. *Elementa: Science of the Anthropocene*, *10*(1), 00060. https://doi.org/10.1525/elementa.2021.00060

Stull, R. B. (1988). *An introduction to boundary-layer meteorology*. Kluwer Academic Publishers.

Sun, J., Mahrt, L., Banta, R. M., & Pichugina, Y. L. (2012). Turbulence regimes and turbulence intermittency in the stable boundary layer during CASES-99. *Journal of the Atmospheric Sciences*, *69*(1), 338–351. https://doi.org/10.1175/JAS-D-11-082.1

Tjernström, M., Balsley, B. B., Svensson, G., & Nappo, C. J. (2009). The effects of critical layers on residual layer turbulence. *Journal of the Atmospheric Sciences*, *66*(2), 468–480. https://doi.org/10.1175/2008jas2729.1

Vercauteren, N., Mahrt, L., & Klein, R. (2016). Investigation of interactions between scales of motion in the stable boundary layer. *Quarterly Journal of the Royal Meteorological Society*, *142*(699), 2424–2433. https://doi.org/10.1002/qj.2835

Xi, X., Yang, Q., Liu, C., Shupe, M. D., Han, B., Peng, S., et al. (2024). Evaluation of the planetary boundary layer height from ERA5 reanalysis with MOSAiC observations over the Arctic Ocean. *Journal of Geophysical Research: Atmospheres*, *129*(12), e2024JD040779. https://doi.org/10.1029/2024JD040779

References From the Supporting Information

Businger, J. A., Wyngaard, J. C., Izumi, Y., & Bradley, E. F. (1971). Flux-profile relationships in the atmospheric surface layer. *Journal of the Atmospheric Sciences*, *28*(2), 181–189. https://doi.org/10.1175/1520-0469(1971)028<0181:FPRITA>2.0.CO;2

Grachev, A. A., Fairall, C. W., Persson, P. O. G., Andreas, E. L., & Guest, P. S. (2005). Stable boundary-layer scaling regimes: The Sheba data. *Boundary-Layer Meteorology*, *116*(2), 201–235. https://doi.org/10.1007/s10546-004-2729-0

Grachev, A. A., Andreas, E. L., Fairall, W. C., Guest, P. S., & Persson, P. O. G. (2013). The critical Richardson number and limits of applicability of local similarity theory in the stable boundary layer. *Boundary-Layer Meteorology*, *147*(1), 51–82. https://doi.org/10.1007/s10546-012-9771-0

Sreenivasan, K. R. (1995). On the universality of the Kolmogorov constant. *Physics of Fluids*, *7*(11), 2778–2784. https://doi.org/10.1063/1.868656